Bachelor Thesis

Landau levels in bilayer quantum spin Hall systems

Bijan Chokoufe Nejad

May 9, 2012

Julius-Maximilians Universität Würzburg

Institut für Theoretische Physik und Astrophysik

Supervisors: Prof. Dr. B. Trauzettel and Dr. P. Michetti

Contents

Acronyms

BHZ	Bernevig, Hughes, and Zhang
DQW	Double quantum well
LL	Landau level
QH	Quantum Hall
QSH	Quantum spin Hall
QW	Quantum well
TRS	Time-reversal symmetry

1 Introduction

The discovery of the topological nature of the quantum Hall (QH) effect [1, 2] led to diffusion of the concept of topology into solid state physics. It turned out that the Hall conductance is in fact given by the first Chern number [3], which assumes integer values only, times the quantum of conductivity e^2/h, independently of material details. A QH system can be indeed understood as a topological phase of matter with broken time-reversal symmetry (TRS) [4] due to the external magnetic field. A new topological phase, the topological insulator phase which preserves TRS, labelled by the Z_2 topological invariant, has been theoretically predicted [5, 6] and experimentally verified [7, 8] in HgTe/CdTe quantum wells (QWs).

The importance of topological insulators for this field of study is underlined by this year's Oliver E. Buckley Prize of the APS: C. Kane (Pennsylvania), L. Molenkamp (Würzburg), and S. Zhang (Stanford) received it *for the theoretical prediction and experimental observation of the QSH effect, opening the field of topological insulators* [9]. In order to find a system which provides an easily controllable topological insulator phase P. Michetti *et al.* proposed a double quantum well (DQW) of HgTe/CdTe layers with interlayer voltage [10]. The voltage allows to tune the system's bandstructure from normal (conventional insulator) into zero-gap (similar to graphene) or inverted (topological insulator). This system allows layer pseudospin-based physics resemblant to that in bilayer graphene with the absence of valley degeneracy. The model can be regarded as a first step to double layer devices which allow to better control spin-polarized edge states and could even be realized with ordinary semiconductor materials like GaAs.

An easy way to experimentally verify the properties of the DQW is to apply a strong magnetic field. The aim of this work is to provide a theoretical calculation of the expected experimental results. The thesis is organized as follows. At first, we give a brief introduction to $\boldsymbol{kp}$ perturbation theory as well as the Peierl's substitution, which is employed to include the influence of an applied magnetic field, in Chapter 2. Then, we use this to review a common model for HgTe/CdTe QWs and it's Landau levels (LLs) in detail in Chapter 3. In particular, we examine the crossing of $n = 0$ LLs at a finite magnetic field as a characterization of the topologically nontrivial systems. In Chapter 4, we apply the same methods to

the DQW. We show that the existence of a crossing leads to the same necessary condition for the interlayer voltage as the existing calculation of the topological invariant in Ref. [10]. Then, we explore the parameter space of the system, varying the tunneling barrier and the thicknesses of the involved layers. Furthermore, we analyze the LLs of a reduced two band model in comparison to the full model. Finally, we summarize the results in Chapter 5 and point out that the experimental verification of this interesting system is within reach.

Acknowledgments

First of all I want to thank Dr. P. Michetti and Prof. Dr. B. Trauzettel for their enduring support on this work. I am grateful for the possibility of working on a topic which is closely related to recent research in solid state physics and the excellent guidance that they provided as supervisors.

Furthermore I want to thank my family for raising and always supporting me and accepting my dedication to physics. Finally I must thank my fellow students and friends of the FOKUS group who encouraged me to push beyond my limits throughout my studies.

2 Theoretical basics of solid state physics

In this chapter, we give a brief summary of the derivation of the basis for models of QSH systems. We assume that, accordingly to the quasi particle picture of electrons, see e.g. Chap. 17 of Ref. [11] and references therein, many body interactions can be absorbed into the effective mass m and the potential $V(\boldsymbol{r})$ which one electron sees. Therefore, we consider the time-independent Schrödinger equation for one electron

$$\mathcal{H}\,|\psi\rangle \equiv \left(\frac{\boldsymbol{p}^2}{2m} + V(\boldsymbol{r})\right)|\psi\rangle = E\;|\psi\rangle \quad \text{with} \quad V(\boldsymbol{r}) = V(\boldsymbol{r}+\boldsymbol{R}) \tag{2.1}$$

like in Ref. [12] where $\boldsymbol{R}$ generates the Bravais lattice and higher relativistic terms of the expansion of the Dirac equation are neglected at first. However, we will later include spin-orbit coupling, $1/(4m^2)(\boldsymbol{\sigma}\times\nabla V)\cdot\boldsymbol{p}$, as a perturbation. Please note that we work in natural units in which

$$\hbar = c = k_\mathrm{B} = 1\;. \tag{2.2}$$

Operator hats are omitted if not absolutely necessary.

2.1 Bloch's theorem and kp perturbation theory

To take advantage of the translational invariance of $\mathcal{H}$ we search for a basis of combined eigenstates with the shift operator $S(\boldsymbol{R})$ since $S(\boldsymbol{R})V(\boldsymbol{r}) = V(\boldsymbol{r}+\boldsymbol{R})$ and $[\mathcal{H}, S(\boldsymbol{R})] = 0$ [13]. This results in the Bloch functions

$$\psi_{\boldsymbol{k}}(\boldsymbol{r}) = \frac{1}{\sqrt{V}}\mathrm{e}^{\mathrm{i}\boldsymbol{k}\boldsymbol{r}}u_{\boldsymbol{k}}(\boldsymbol{r}) \quad \text{with} \quad u_{\boldsymbol{k}}(\boldsymbol{r}+\boldsymbol{R}) = u_{\boldsymbol{k}}(\boldsymbol{r}) \tag{2.3}$$

where we have used periodic boundary conditions and restricted the crystal momentum $\boldsymbol{k}$ to the first Brillouin zone [12]. Since $\boldsymbol{p}$ in Eq. (2.1) acts on both factors in Eq. (2.3) we get additional terms due to the product rule if we rewrite Eq. (2.1)

for the $u_{\boldsymbol{k}}(\boldsymbol{r})$ for each $\boldsymbol{k}$:

$$\left[\frac{\boldsymbol{p}^2}{2m} + V(\boldsymbol{r}) + \frac{1}{m}\boldsymbol{k}\boldsymbol{p} + \frac{\boldsymbol{k}^2}{2m}\right] u_{n\boldsymbol{k}}(\boldsymbol{r}) = E_n(\boldsymbol{k}) u_{n\boldsymbol{k}}(\boldsymbol{r})\,. \tag{2.4}$$

This is now a boundary value problem in the unit cell with $\boldsymbol{k}$ as parameter [12]. Here, we have introduced the band index n because we expect discrete eigenvalues $E_n(\boldsymbol{k})$ for this problem. n can also include the two spin components. The third term in Eq. (2.4) is at the origin for the $\boldsymbol{kp}$ method which has been summarized by Kane in 1966 [14]. The general idea is to determine the bands by using known wave functions at a certain point $\boldsymbol{k}_0$, e.g. the Γ point $\boldsymbol{k}_0 = 0$. In fact, it is convenient to chose an high symmetry point of the Brillouin zone [15]. Since for any $\boldsymbol{k}_0$ the functions $u_{n\boldsymbol{k}_0}(\boldsymbol{r}) = \langle r \mid n\boldsymbol{k}_0\rangle$ $(n = 0, 1, 2, \dots)$ form a complete set, we can change the basis:

$$u_{n\boldsymbol{k}}(\boldsymbol{r}) = \sum_{n'} \left\langle r \,\middle|\, n'\boldsymbol{k}_0 \right\rangle \left\langle n'\boldsymbol{k}_0 \,\middle|\, n\boldsymbol{k} \right\rangle \equiv \sum_{n'} c_{n'n}(\boldsymbol{k}) u_{n'\boldsymbol{k}_0}(\boldsymbol{r})\,. \tag{2.5}$$

By multiplying Eq. (2.4) by $u_{n\boldsymbol{k}_0}$ and substituting Eq. (2.5) into it we obtain:

$$\sum_{n'} \left[\left(E_n(\boldsymbol{k}_0) + \frac{1}{2m}(\boldsymbol{k}^2 - \boldsymbol{k}_0^2)\right)\delta_{nn'} + \frac{1}{m}(\boldsymbol{k} - \boldsymbol{k}_0)\left\langle n\boldsymbol{k}_0 \,\middle|\, \boldsymbol{p} \,\middle|\, n'\boldsymbol{k}_0 \right\rangle\right] c_{n'n} = E_n(\boldsymbol{k}) c_{nn} \tag{2.6}$$

which is also known as $\boldsymbol{k}_0$ representation and is correct so far for any $\boldsymbol{k}$. However if $\boldsymbol{k}$ is near $\boldsymbol{k}_0$ we may treat the nondiagonal part of Eq. (2.6) as perturbation. The $\boldsymbol{kp}$ method heavily relies on symmetry considerations because this reduces the number of off-diagonal terms which one has to calculate. This is why we have to consider the symmetry of zinc blende structures in Section 3.1 before we continue with Eq. (2.6).

2.2 Peierl's substitution

Since this thesis is focused on the LLs of QSH systems, we have to translate the known minimal coupling for electrons $\boldsymbol{p} \to \boldsymbol{p} + e\boldsymbol{A}$ $(e > 0)$, see e.g. Ref. [16], to the resulting model which will only consist of $\boldsymbol{k}$. Luttinger and Kohn (LK) included this discussion in Ref. [17]. In order to be concrete we use an explicit gauge $\boldsymbol{A} = (-\mathcal{B}y, 0, 0)$ which produces a magnetic field in z direction. If we apply

the coupling to Eq. (2.1) we get two additional terms

$$\mathcal{H} \to \mathcal{H} + \frac{e\mathcal{B}}{m} y p_x + \frac{(e\mathcal{B})^2}{2m} y^2 \,. \tag{2.7}$$

With the product rule for the Bloch functions we get two terms for p_x, like in Eq. (2.4), when we rewrite the Hamiltonian for the $u_{\boldsymbol{k}}$. In order to remove the off-diagonal interband parts of Eq. (2.6) to first order, LK apply a canonical transformation T. This can be written as:

$$\begin{aligned} HA = \epsilon A, \qquad & TA \equiv \mathrm{e}^{S} A = B. \\ \Rightarrow \mathrm{e}^{S} H \mathrm{e}^{-S} B = \epsilon B, \qquad & \text{and} \\ \mathrm{e}^{S} H \mathrm{e}^{-S} = H + [S, H] + \frac{1}{2} [S, [S, H]] + .. & \end{aligned} \tag{2.8}$$

which can be seen by simple power expansion or by use of the Hadamard lemma: $e^X Y e^{-X} = e^{\mathrm{ad}_X} Y$, $\mathrm{ad}_X\, Y \equiv [X, Y]$ [18]. If we think of Eq. (2.6) as $H = H^0 + H^1$ where H^0 are the diagonal parts and H^1 the off-diagonal, we can choose S so $H^1 + \left[S, H^0\right] = 0$. This eliminates the interband elements to first order and so LK arrive at a effective mass theory with one band [17]. By calculating the matrix elements of S, one can conclude that due to the involved variables they are of the order of a/l_B, where a is the lattice spacing and $l_B = 1/\sqrt{e\mathcal{B}}$ is the magnetic length. The estimated error made by dropping higher order terms of S is of the order of $(a/l_B)^2$. Finally, LK outline that it is equivalent to replace $\boldsymbol{k} \to -\mathrm{i}\nabla + e\boldsymbol{A}$, if one is interested in the band structure up to second order. When doing so any product of noncommuting factors should be symmetrized. This is called Peierl's substitution [19]. Although this derivation is made for a one band model, a similar argumentation should be possible for the multiband $\boldsymbol{kp}$ description that we use later on. Hereby, one should remove the additional off-diagonal terms coming from Eq. (2.7) and keep only the off-diagonal terms which don't arise from the magnetic field but are wanted in the multiband model.

3 Zincblende quantum wells

Kane's analysis of the band structure of InSb [20] can be also applied to HgTe or CdTe since all of them have a crystal structure of the zincblende type. This chapter gives a overview of possible bases, models, and finally the LLs of these structures.

3.1 Tetrahedral group T_d

Zincblende structures can be seen as two interpenetrating face-centered cubic lattices, i.e. like diamond but with different atoms. Each atom has four nearest neighbor atoms of the opposite type and these form a regular tetrahedron. The corresponding symmetry group is the tetrahedral group T_d which is a subgroup of the full octahedral group O_h. The missing symmetry element is the inversion due to different atoms. This lifts the degeneracy of spin up and down for a finite k. However the influence of this microscopic inversion asymmetry has been examined and seems to have negligible effects in HgTe/CdTe QWs [21]. From group theory we know the symmetry properties of the $u_{n\mathbf{0}}$ which we use as basis. They should transform under an irreducible representation Γ_α of the point group of the crystal. For example $|S\uparrow\rangle$ and $|S\downarrow\rangle$ have s-like symmetry properties under the operations of the tetrahedral group [20]. On the other hand, there are p-like functions like $|X\uparrow\rangle$,$|X\downarrow\rangle$, $|Y\uparrow\rangle$,$|Y\downarrow\rangle$, $|Z\uparrow\rangle$, and $|Z\downarrow\rangle$. In order to account for the spin-orbit coupling, which is strong in HgTe [7], we can take a basis $|\Gamma_\alpha, m_j\rangle$ in which it is diagonal:

$$
\begin{aligned}
\left|\Gamma_6, +\frac{1}{2}\right\rangle &= |S\uparrow\rangle\,, \\
\left|\Gamma_6, -\frac{1}{2}\right\rangle &= |S\downarrow\rangle\,, \\
\left|\Gamma_8, +\frac{3}{2}\right\rangle &= \frac{1}{\sqrt{2}}\Big(|X\uparrow\rangle + \mathrm{i}\,|Y\uparrow\rangle\Big), \\
\left|\Gamma_8, +\frac{1}{2}\right\rangle &= \frac{1}{\sqrt{6}}\Big(|X\downarrow\rangle + \mathrm{i}\,|Y\downarrow\rangle - 2\,|Z\uparrow\rangle\Big),
\end{aligned}
$$

$$
\begin{aligned}
\left|\Gamma_8, -\frac{1}{2}\right\rangle &= -\frac{1}{\sqrt{6}}\Big(|X\uparrow\rangle - \mathrm{i}\,|Y\uparrow\rangle + 2\,|Z\downarrow\rangle\Big),\\
\left|\Gamma_8, -\frac{3}{2}\right\rangle &= -\frac{1}{\sqrt{2}}\Big(|X\downarrow\rangle - \mathrm{i}\,|Y\downarrow\rangle\Big),\\
\left|\Gamma_7, +\frac{1}{2}\right\rangle &= \frac{1}{\sqrt{3}}\Big(|X\downarrow\rangle + \mathrm{i}\,|Y\downarrow\rangle + |Z\uparrow\rangle\Big), \quad \text{and}\\
\left|\Gamma_7, -\frac{1}{2}\right\rangle &= \frac{1}{\sqrt{3}}\Big(|X\uparrow\rangle - \mathrm{i}\,|Y\uparrow\rangle - |Z\downarrow\rangle\Big).
\end{aligned} \tag{3.1}
$$

This can be found in [14, 21] and is the basis for the 8x8 Kane Hamiltonian. $m_j = \pm(3/2, 1/2)$ refers to the total angular momentum $J = L \oplus S$ which is formed by ordinary spin addition of the angular momentum L in the unit cell and the spin of the electron S. However, the sign of this total angular momentum will often be loosely referred to as spin up or down in the remainder of this thesis as usually done in the related literature. The matrix elements of the Kane Hamiltonian are basically given by Eq. (2.6) for $\boldsymbol{k}_0 = \mathbf{0}$. Due to the symmetry of Eq. (3.1) one can conclude if they have to contain k_x, k_y, k_z or $k_\pm = k_x \pm \mathrm{i}k_y$. By using this basis the most accurate results can be expected but it is quite cumbersome to handle. Γ_7 is also called split-off band since it is energetically seperated from the other bands. Because it has negligible effects on the band structure (smaller than 5 % [21]), one might drop it and arrive at the 6x6 Kane Hamiltonian. As we can see in Fig. 3.1, CdTe has the so called *normal* band structure with $|\Gamma_6, m_j\rangle$ above $|\Gamma_8, m_j\rangle$ while bulk HgTe has an *inverted* bandstructure, where the conduction band has p character. Bulk should indicate here that we have a macroscopic solid state and no QW structure which can have a quite different band structure.

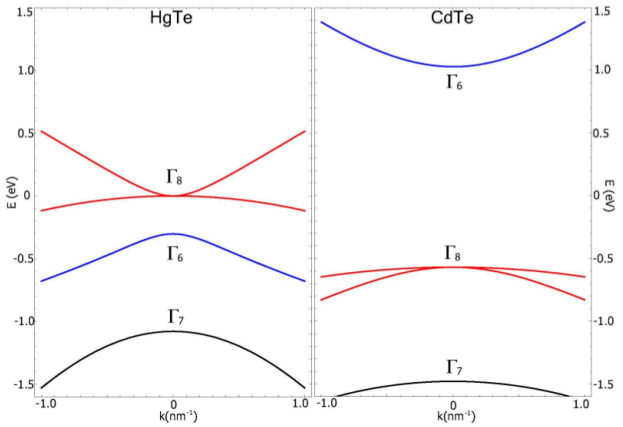

Figure 3.1: Bandstructure of HgTe and CdTe. From Ref. [7].

3.2 Heterostructures

If we think of a QW, which consists basically of a thin layer with a width of about three to 20 nanometres in between two other layers of different material, it is clear that the Bloch functions in Eq. (2.3) have to be modified. k_z is no more a conserved quantity and the generalized ansatz can be written as [22]

$$\psi(\boldsymbol{r}) = \sum_n F_n(\boldsymbol{r}) u_n(\boldsymbol{r}) \quad \text{with} \quad F_n(\boldsymbol{r}) = \mathrm{e}^{\mathrm{i}(k_x x + k_y y)} f_n(z)\,. \tag{3.2}$$

$F_n(\boldsymbol{r})$ are known as envelope functions and this approach has been introduced by Burt [23]. As noted before Γ_7 can be neglected. Due to the left axial rotation symmetry m_j is for $\boldsymbol{k}_\parallel = (k_x, k_y) = \boldsymbol{0}$ still a good quantum number [6]. Furthermore, when we later apply a magnetic field in the z direction, m_j will still be a conserved quantity. In the following, we concentrate on HgTe/CdTe QWs which realize the experimentally most accessible QSH phase. As shown in Ref. [21], the left six bands of Eq. (3.1) form QW subbands where the ones nearest to the neutrality point are E1, H1, and L1. E,H, and L refers to electron, heavy-hole and light-hole. However, this notation should not be taken too seriously since the dispersion of them depends heavily on the QW width [21]. L1 is seperated from the other two and might be neglected as well [7]. Then, we are left with

$$\begin{aligned} |E1,\pm\rangle &= \alpha \left|\Gamma_6, \pm\frac{1}{2}\right\rangle + \beta \left|\Gamma_8, \pm\frac{1}{2}\right\rangle \quad \text{and} \\ |H1,\pm\rangle &= \left|\Gamma_8, \frac{3}{2}\right\rangle, \end{aligned} \tag{3.3}$$

which can mix away from the Γ point. Now one can calculate the matrix elements

$$H_{ij}(k_x, k_y) = \int \mathrm{d}z\ \langle \psi_j \,|\, H_{6x6}(k_x, k_y, -\mathrm{i}\partial_z) \,|\psi_i\rangle\,, \tag{3.4}$$

where H_{6x6} refers to the Kane model and $|\psi_i\rangle$ to the basis in Eq. (3.3). A different approach is to consider the symmetry of this basis to conclude which terms should be included in the model. Because of the rotational symmetry along z, the lowest nontrivial coupling terms between $|E\pm\rangle$ and $|H\pm\rangle$ are proportional to $k_\pm$. The diagonal terms should be even under parity, so we allow constant and quadratic terms there. Furthermore, we restrict ourselves to a model which doesn't split the degeneracy of $\pm$ induced by TRS T. An explicit consideration of this symmetry

will be later given in Section 4.1. Due to Bernevig, Hughes, and Zhang who have introduced this effective 4x4 Hamiltonian [6], we call this the BHZ model:

$$\begin{aligned} H_{\mathrm{BHZ}}(\boldsymbol{k}) &= \begin{pmatrix} h(\boldsymbol{k}) & \\ & h^*(-\boldsymbol{k}) \end{pmatrix}, \\ h(\boldsymbol{k}) &= \boldsymbol{d}\cdot\boldsymbol{\sigma} \equiv d_0\sigma_0 + d_1\sigma_1 + d_2\sigma_2 + d_3\sigma_3\,, \\ \boldsymbol{d} &= (C - D\boldsymbol{k}_\parallel^2, Ak_x, -Ak_y, M - B\boldsymbol{k}_\parallel^2)\,. \end{aligned} \tag{3.5}$$

The ordered basis is $|E1+\rangle$, $|H1+\rangle$, $|E1-\rangle$ and $|H1-\rangle$. The Pauli matrices σ correspond to the band pseudospin $E1$ and $H1$. The most important parameter in this model is the Dirac mass M. For $M < 0$, Eq. (3.5) describes the inverted band structure of the two bands of HgTe, we are interested in. For $M > 0$, we get the normal ordering of the bands which corresponds to CdTe or a very thin QW of HgTe with $d < d_c$. d_c is the critical thickness which relates to $M = 0$ in the model above [6]. In the following, we set C=0 which only plays the role of an offset in energy. $h(\boldsymbol{k})$ can also be written in terms of $k_\pm$

$$h(\boldsymbol{k}) = \begin{pmatrix} M - \frac{D+B}{2}(k_+k_- + k_-k_+) & Ak_+ \\ Ak_- & -M - \frac{D-B}{2}(k_+k_- + k_-k_+) \end{pmatrix}. \tag{3.6}$$

We have symmetrized k_+k_- because it will become a product of non-commuting factors in the next section.

3.3 Landau levels

We employ the Peierl's substitution which has been shown in Section 2.2,

$$\boldsymbol{k} \to \boldsymbol{\pi} = \boldsymbol{k} + e\boldsymbol{A}, \tag{3.7}$$

where $\boldsymbol{k}$ has to be regarded as $-\mathrm{i}\nabla$, to study the LLs of this system. We have seen that this substitution for $\boldsymbol{k}$ is valid as long as the lattice spacing $a \ll l_B = 1/\sqrt{e\mathcal{B}}$. For HgTe and CdTe $a \approx 0.65\,\mathrm{nm}$ [24] while $l_B > 8.11\,\mathrm{nm}$ for magnetic fields up to $\mathcal{B} = 10\,\mathrm{T}$. So the error $(a/l_B)^2$ is negligible. In the remainder of this thesis, the Zeeman splitting $\Delta_Z = g\mu_B B$ won't be taken into account as we want to concentrate on the orbital degrees of freedom. This yields the characteristic band structure of electrons in a magnetic field [25] due to the relatively

small $\mu_B = 5.788 \times 10^{-5}\,\mathrm{eV\,T^{-1}}$. For a magnetic field $\boldsymbol{\mathcal{B}}$ in the growth direction of the heterostructure [001], i.e. z, we can choose the symmetric gauge $\boldsymbol{A} = \mathcal{B}/2(-y, x, 0)$. Hence we get

$$\begin{aligned} k_+ \to \pi_+ &= k_+ + \mathrm{i}\frac{e\mathcal{B}}{2}(x + \mathrm{i}y)\,, \\ k_- \to \pi_- &= k_- - \mathrm{i}\frac{e\mathcal{B}}{2}(x - \mathrm{i}y) \end{aligned} \tag{3.8}$$

Since we have integrated out the spatial z degree of freedom, we have a two-dimensional system as long as we are only interested in the lowest bands. By using the well-known commutator relation $[x_i, k_j] = \mathrm{i}\delta_{ij}$ we obtain

$$\begin{aligned} [\pi_+, \pi_-] &= \frac{\mathrm{i}}{2l_B^2}\Big(\big[k_+, -(x - \mathrm{i}y)\big] + \big[x + \mathrm{i}y, k_-\big]\Big) \\ &= -\frac{2}{l_B^2} \qquad \text{and} \\ [\pi_+, \pi_+] &= 0 = [\pi_-, \pi_-]\,. \end{aligned} \tag{3.9}$$

This is already the commutator algebra of the harmonic oscillator which can be normalized by introduction of the corresponding ladder operators:

$$a = \frac{l_B}{\sqrt{2}}\pi_- \quad \Rightarrow \quad a^\dagger = \frac{l_B}{\sqrt{2}}\pi_+\,. \tag{3.10}$$

The Hamiltonian in Eq. (3.6) takes the form

$$h(\boldsymbol{k}) \to h_+ = \begin{pmatrix} M - \frac{2(D+B)}{l_B^2}(a^\dagger a + \frac{1}{2}) & \frac{\sqrt{2}A}{l_B}a^\dagger \\ \frac{\sqrt{2}A}{l_B}a & -M - \frac{2(D-B)}{l_B^2}(a^\dagger a + \frac{1}{2}) \end{pmatrix}. \tag{3.11}$$

If we recall the effect of the ladder operators on a bosonic Fock state $|n\rangle \in F_\nu(H)$, $a^\dagger a\,|n\rangle = n\,|n\rangle$, $a\,|n\rangle = \sqrt{n}\,|n-1\rangle$ and $a^\dagger\,|n\rangle = \sqrt{n+1}\,|n+1\rangle$ [26], we can see that a finite number of LLs are coupled. The second block of Eq. (3.5) $h^*(-\boldsymbol{k}) \to h_-$ has the same diagonal elements and the negative complex conjugate on the offdiagonal. Since the two blocks h_+ and h_- are decoupled we can solve them independently. We make an ansatz for $n > 0$

$$|\psi_+\rangle = \begin{pmatrix} e_+\,|n\rangle \\ h_+\,|n-1\rangle \end{pmatrix} \quad \text{and} \quad |\psi_-\rangle = \begin{pmatrix} e_-\,|n-1\rangle \\ h_-\,|n\rangle \end{pmatrix} \tag{3.12}$$

which is obviously an eigenvector with respect to the ladder operators. This leads to two algebraic symmetric matrices

$$h_\pm |\psi_\pm\rangle = \begin{pmatrix} M - \frac{2(D+B)}{l_B^2}(n \pm \frac{1}{2}) & \pm\frac{\sqrt{2}A}{l_B}\sqrt{n} \\ \pm\frac{\sqrt{2}A}{l_B}\sqrt{n} & -M - \frac{2(D-B)}{l_B^2}(n \mp \frac{1}{2}) \end{pmatrix} |\psi_\pm\rangle \tag{3.13}$$

which can be easily solved. Because we break the TRS of the system with the applied, external magnetic field, we can expect different energies for the two blocks which used to be degenerated. The eigenvalues are

$$E_\alpha^{1/2} = \frac{1}{l_B^2}(-\alpha B - 2Dn) \pm \sqrt{\left(M - \frac{2}{l_B^2}\left(nB + \alpha\frac{D}{2}\right)\right)^2 + \frac{2A^2 n}{l_B^2}} \tag{3.14}$$

where $\alpha = \pm$ corresponds to the two blocks, i.e. spin up or spin down. This result has also been found by König *et al.* [7]. Since $1/l_B^2 \propto \mathcal{B}$ we can see that the LLs have a linear and a square root $\mathcal{B}$ term. Let us compare this with other known results. The LLs of a free electron gas $E = \omega_c(n + 1/2)$ are linear in $\mathcal{B}$ because $\omega_c = e\mathcal{B}/m$ [26]. The relativistic LLs of graphene disperse as $\sqrt{\mathcal{B}n}$ [25]. This behaviour is included in this model for the case $B = D = M = 0$. More generally if only M equals zero we have the case of a zero-gap HgTe QW. This case is also experimentally accessible by growing QWs with the critical thickness of $d_C \approx 6.3\,\text{nm}$. Fig. 3.2 shows good agreement of the calculated LLs of the BHZ model with the experimental fan charts for $n = 0, 1, 2$. Especially the linear dispersion of the zero modes is verified. For higher LLs the BHZ model can't reproduce the accuracy of the 8-band $\boldsymbol{k}\cdot\boldsymbol{p}$ Kane model and remains only valid for small magnetic fields.

3.4 Zero modes

For Landau level index $n = 0$, we find the following eigenvectors

$$|\psi_+\rangle = \begin{pmatrix} |0\rangle \\ 0 \end{pmatrix} \quad \text{and} \quad |\psi_-\rangle = \begin{pmatrix} 0 \\ |0\rangle \end{pmatrix}, \tag{3.15}$$

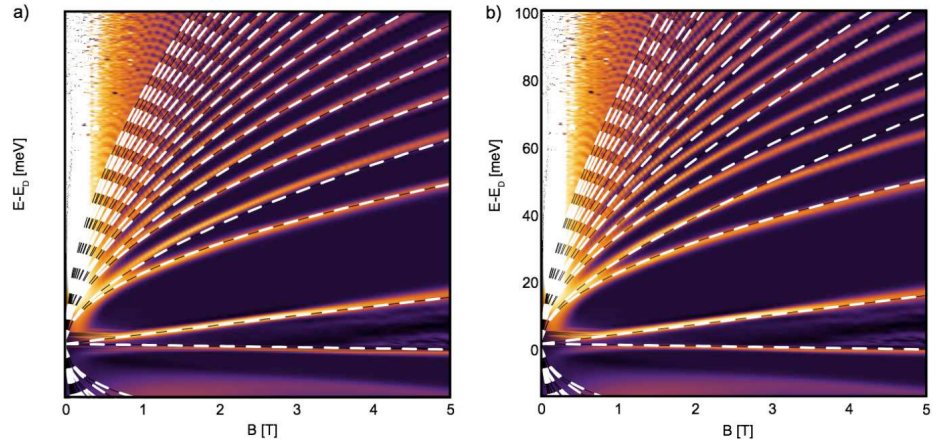

Figure 3.2: Experimental LL fan charts by plotting $\partial\sigma_{xy}/\partial V_{\mathrm{Gate}}$. The dashed lines are calculations with a) the 8-band ***kp*** model and b) the BHZ model. From Ref. [27].

with eigenenergies ($\alpha = \pm$)

$$E_\alpha^0 = \alpha M - \frac{(D + \alpha B)}{l_B^2}\,. \tag{3.16}$$

The fact that for spin up (down) only an E1 (H1) component is allowed, results from the operator structure of Eq. (3.11) and will also be the case for the DQW. So the zero modes are described by two lines with respect to $\mathcal{B}$ which cross eventually. The energy splitting between them is given by $E_+^0 - E_-^0 = 2M - 2B/l_B^2$. By setting this to zero we obtain a crossing field

$$\mathcal{B}_c = M/(Be) \tag{3.17}$$

for which the two energies Eq. (3.16) become degenerate. We can see now that only in the inverted regime $M/B > 0$ ($B, M < 0$) there is a finite crossing point. The crossing point of the lowest LLs has proven to be a precise measure of well thickness [27]. For a given magnetic field the Hall conductivity σ_{xy} can be measured by varying the gate voltage as shown in fig. 2 of [27]. By using this method Eq. (3.16) can be measured as the energies at which σ_{xy} jumps from 0 to $\pm e^2/h$. This behaviour will be discussed later on in more detail. Typical values for the parameters of the BHZ model are given in Table 3.1. For the inverted regime, we can set $M = -M_0$ which gives qualitatively the same result as the set of parameters used in Ref. [27]. In Fig. 3.4 the LLs are plotted for the normal and the inverted regime. Since E1 and H1 bands are coupled, the eigenvectors of the

A_0 [eV nm]	B_0 [eV nm^2]	D_0 [eV nm^2]	M_0 [eV]
0.375	-1.120	-0.730	0.0065

Table 3.1: Values from [10] for a HgTe-QW with thickness d=5.7 nm.

system for a given $\mathcal{B}$ may be a mixture of E1 and H1. In Fig. 3.5, we can see that for $\mathcal{B} = 0$ the eigenvectors are either of E1 or H1 type. While for the normal bandstructure the eigenvectors keep their dominant character, this is not the case for the inverted regime. In fact they swap their roles for a certain $\mathcal{B}_S$. By putting the ratio of the weights of Eq. (3.12) $q \equiv |e_\pm|^2/|h_\pm|^2 = 1$, we obtain

$$\mathcal{B}_S = \frac{M}{e(\pm D + 2Bn)}, \tag{3.18}$$

where $\pm$ is for spin up and down. For the relevant parameters $\mathcal{B}_S < 1.5\,\mathrm{T}$, so this should be imporant even for small fields. The qualitative behaviour of the ratio plot in Fig. 3.5 is the same for all n and all considered parameters. This swapping is not too surprising if we think of the $E(\boldsymbol{k})$ dispersion. Like it is shown in Fig. 3.3, for $d < d_c$ the lower band is dominantly $H1$ and the upper one $E1$. For $d > d_c$, i.e. the inverted regime, and $\boldsymbol{k}_\parallel = 0$ the bands have flipped their character but swap back to the $d < d_c$ case for large $\boldsymbol{k}_\parallel$. So this feature is inherited to the LLs since we are coupling $\mathcal{B}$ with $\boldsymbol{k}$ in Eq. (3.8).

However, the zero modes are not affected by this mixing at all. By a simple look at Eq. (3.15), we can see that the E1 (H1) eigenvector won't change their character ever. This is why the argumentation of Ref. [7] holds if the Fermi energy ϵ_F is close to the crossing point although the authors haven't mentioned the mixing at all. So let's have a closer look at the crossing which appears only in an inverted band structure as mentioned before. In order to understand the behaviour of this QW, we have to keep in mind that it is embedded in a material with normal band structure, e.g. CdTe. Therefore, the bands of the inverted regime become normal, i.e. E1 over H1 band, at the edges of the system. We can see from Fig. 3.4 that for $\mathcal{B} > \mathcal{B}_c$, the band structure has already the normal order. If we put the chemical potential between the zero modes the QW acts as an ordinary, so called *topologically trivial*, insulator.

For a fixed $\mathcal{B} < \mathcal{B}_c$, the bands have to cross ϵ_F in order to get to the normal ordering at the edge and therefore allow two possible edge channels. As mentioned before,

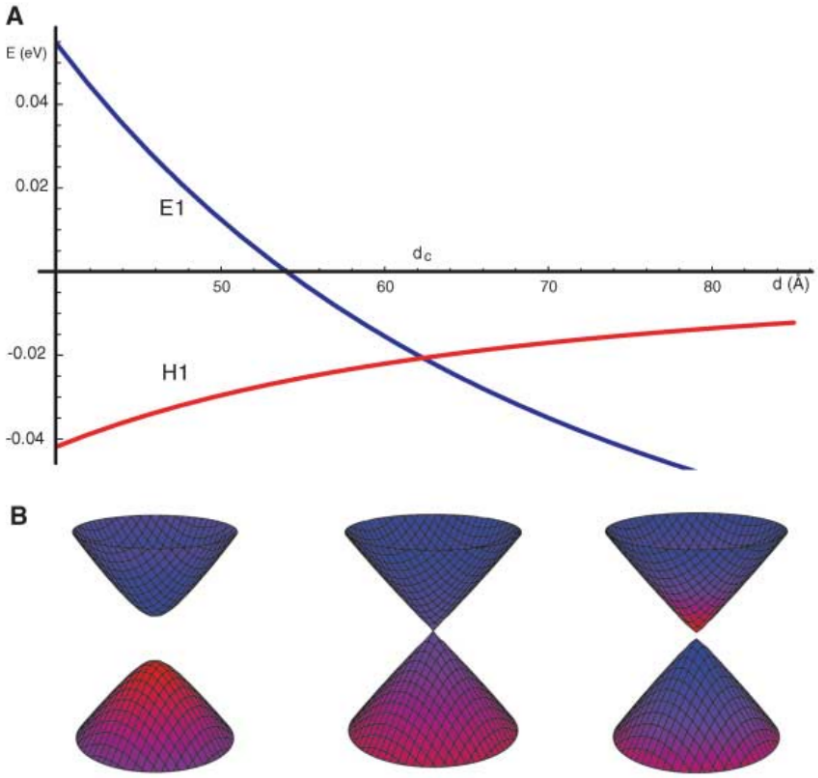

Figure 3.3: In A the energy of E1 and H1 bands at $\boldsymbol{k}_{\parallel} = 0$ is shown as function of the QW thickness. B shows energy dispersions for $d = 4\,\text{nm}$, $6.35\,\text{nm}$ and $9\,\text{nm}$. The color shading indicates the symmetry type where blue corresponds to E1 and red to H1. One can see that in the inverted regime, $d > d_c$, a swapping of the symmetry character occurs. From Ref. [6].

these are not coupled and from Eq. (3.15) we can see that they have opposite spin (indicated by $\pm$). By remembering that $\uparrow$ and $\downarrow$ correspond to $\boldsymbol{k}$ and $-\boldsymbol{k}$ through TRS, this gives rise to the picture of the QSH effect with counter-propagating edge states. This behaviour is called the *topologically nontrivial* regime [6]. A real understanding of the topological features would go beyond the scope of this thesis and we only keep in mind that nontrivial corresponds to an inverted band structure in our system and is indicated by a crossing of zero modes. Finally, there are two interesting cases left with $\mathcal{B} \approx \mathcal{B}_c$ and ϵ_F slightly above or below the crossing point. In these cases only one of the bands crosses ϵ_F. This single edge state is similar to the well known QH regime and the resulting Hall conductance changes sign for the two cases due to the opposite propagation direction of the two zero modes.

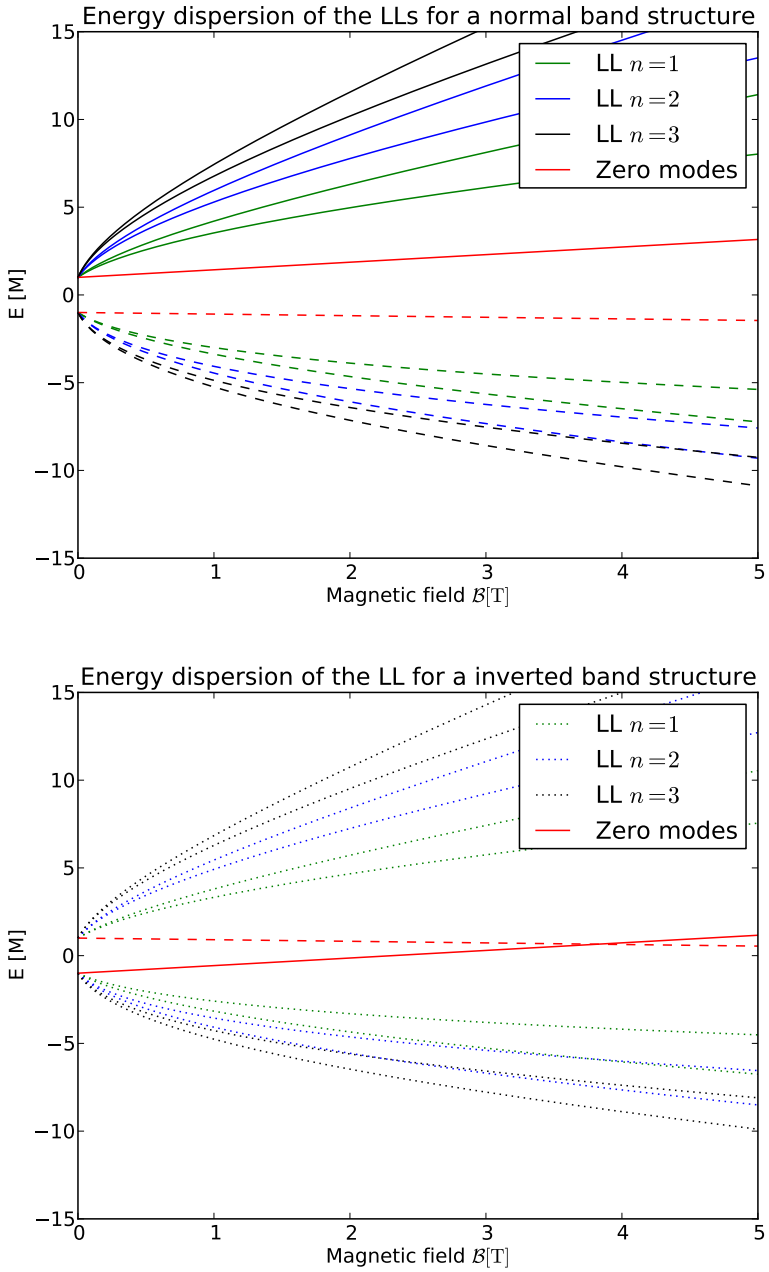

Figure 3.4: The energy dispersion by using the parameters in Table 3.1 and $M = \pm M_0$. Dashed (solid) lines represent LLs which have predominantly H1 (E1) character, see also Fig. 3.5 and remarks in the text. Dotted lines are strongly mixed states.

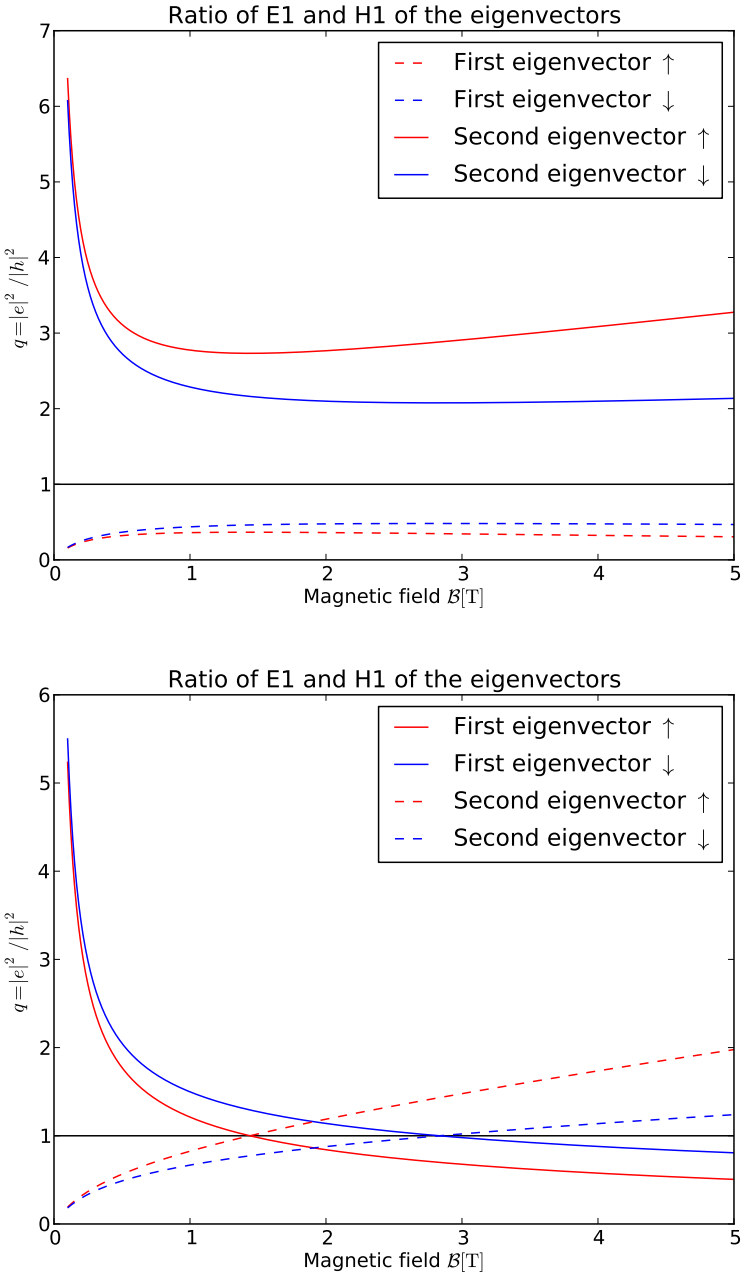

Figure 3.5: The ratio determines E1 or H1 character. For $q \to \infty$ the eigenvector is equal to E1 for $q \to 0$ to H1. $q = 1$ represents equal weight of E1 and H1. We can see that the E1 and H1 states mix when the magnetic field is turned on. The upper (lower) figure corresponds to normal (inverted) band structure for $n = 1$. Higher LLs look similar.

4 Double Quantum Well

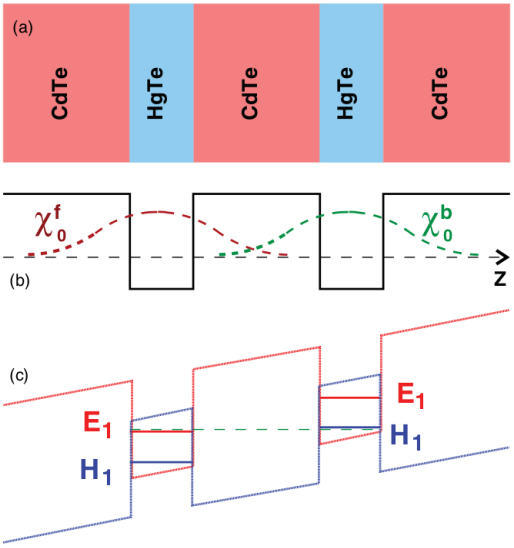

Figure 4.1: a) Schematic representation of the HgTe/CdTe with the upper and lower layer. b) The finite overlap of the individual envelope functions of the layers results in the tunneling parameters α and Δ_{E1E1}. c) Process of band inversion caused by the applied potential V. From Ref. [10].

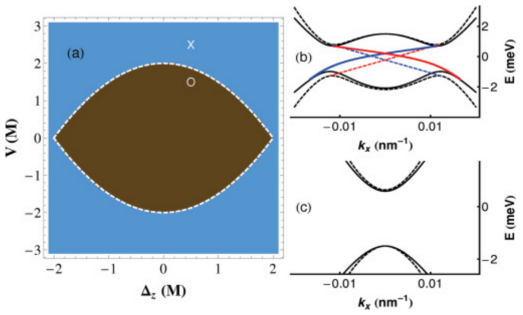

Figure 4.2: a) Calculated Kramers Chern number of a DQW with $\Delta_{H1H1} \approx 0$. The dashed line is obtained with Eq. (4.4). The system is topologically trivial in the inner region (black), but can be driven into the nontrivial regime (blue) with an appropriate voltage V. b) and c) Conduction and valence bands are drawn black. Full (dashed) lines represent solutions obtained by the full (reduced) model. The edge state dispersion curves (blue and red) are calculated by accounting for the boundary conditions. The used layer and tunneling parameters are $M = 6\,\text{meV}$, $\Delta_{E1E1} = 6\,\text{nm}$, and $\alpha = 5\,\text{nm}$. b) and c) correspond to the blue and black regime in a), respectively. From Ref. [10].

Let us introduce the concept of a DQW. For simplicity, a symmetric structure is assumed which means that two HgTe QWs of the same thickness d are separated by a barrier of width t. Michetti *et al.* have shown that, to first order in k, this system can be described as two BHZ models coupled by a tunneling Hamiltonian [10]

$$\begin{aligned} H_T &= +\frac{1}{2}(\boldsymbol{\Delta}\cdot\boldsymbol{\sigma})\mathcal{P}_1\,, \\ \boldsymbol{\Delta} &= (\Delta_0, \alpha k_x, -\alpha k_y, \Delta_z)\,, \end{aligned} \tag{4.1}$$

where $\mathcal{P}_\alpha$ are Pauli matrices associated with the layer pseudospin of the upper and lower layer. So, one should read Eq. (4.1) as coupling matrix between the layers which is caused by a finite overlap of their envelope functions, as indicated

in Fig. 4.1. The diagonal blocks are described by the BHZ model $h(\boldsymbol{k})$ which we have reviewed in the last chapter. As pointed out in Ref. [10], we consider $\boldsymbol{\Delta}$ to be real. The basis is the same as in Section 3.2 for the upper (U) and the lower (L) layer, respectively, but for simplicity we only regard one Kramer's pair, e.g. spin up, at first. Eq. (4.1) can then be explicitly written as

$$\boldsymbol{\Delta}\cdot\boldsymbol{\sigma} = \begin{pmatrix} \Delta_0+\Delta_z & \alpha k_+ \\ \alpha k_- & \Delta_0-\Delta_z \end{pmatrix} \equiv \begin{pmatrix} \Delta_{E1E1} & \Delta_{E1H1} \\ \Delta_{H1E1} & \Delta_{H1H1} \end{pmatrix} . \tag{4.2}$$

Similar to the BHZ model the coupling between E1 and H1 is, due to the symmetry of the wave functions, proportional to $k_\pm$. A convenient control parameter for a bilayer system is a potential V which allows to control the energy gap between the two layers. By including this, we obtain the DQW-BHZ model for a single Kramer's block

$$\begin{aligned} H^{\uparrow} &= (\boldsymbol{d}\cdot\boldsymbol{\sigma})\,\mathcal{P}_0 + \frac{1}{2}(\boldsymbol{\Delta}\cdot\boldsymbol{\sigma})\,\mathcal{P}_1 \; + \frac{V}{2}\sigma_0\,\mathcal{P}_3 \\ &= \begin{pmatrix} \boldsymbol{d}\cdot\boldsymbol{\sigma} + \frac{V}{2}\,\sigma_0 & +\frac{1}{2}(\boldsymbol{\Delta}\cdot\boldsymbol{\sigma}) \\ +\frac{1}{2}(\boldsymbol{\Delta}\cdot\boldsymbol{\sigma}) & \boldsymbol{d}\cdot\boldsymbol{\sigma} - \frac{V}{2}\,\sigma_0 \end{pmatrix} . \end{aligned} \tag{4.3}$$

This DQW has very interesting properties. As shown in Fig. 4.2 the topological insulator phase is depending on the voltage V and therefore, two individually trivial layers can be coupled to a system with a nontrivial QSH phase. The mentioned reduced model in Fig. 4.2 will be discussed in Section 4.5 with an emphasis on the LLs. In order to find the possible topological phase transition, the authors of Ref. [10] searched for an inversion of bands with E1 and H1 character at the $\Gamma-$point and derived:

$$V_c^2 = \frac{1}{4M^2}\left[\left(4M^2 - \frac{\Delta_0^2+\Delta_z^2}{2}\right)^2 - \frac{\left(\Delta_0^2-\Delta_z^2\right)^2}{4}\right] . \tag{4.4}$$

This model is sufficient as long as there is no magnetic field because the energies of the spin up and down block are degenerate due to TRS. As mentioned in Section 3.2, an applied magnetic field breaks this symmetry. Therefore we have to consider both Kramer's blocks to obtain all energy levels.

4.1 Time-reversal symmetry

We know from quantum field theory, to be exact due to Wigner's theorem and some considerations like in Section 2.6 in Ref. [28], that TRS acts as an antilinear and antiunitary transformation T in the Hilbert space. A common representation is to write $T = UK$ with a unitary operator U and K as operator of complex conjugation so we don't have to keep in mind that T is antiunitary, see Section 4.4 of Ref. [29]. In a spinor basis, we also have to account for the spin-reversal due to T which can be realized by σ_2 in the spinor space. Furthermore, we want to assure the crucial relation $T^2 = -1$ [29] as we have only half-integer spin bands included ($j = 1/2, 3/2$). The band pseudospin however shouldn't be affected by T, so T should be proportional to σ_0 in the pseudospin space.

In total we obtain $T_{4\text{x}4} = \mathrm{i}\,(\sigma_2 \otimes \sigma_0)\,K$ where the Kronecker product is denoted by $\otimes$. The order corresponds to the chosen basis $|E1+\rangle$, $|H1+\rangle$, $|E1-\rangle$ and $|H1-\rangle$. In order to apply this $T_{4\text{x}4}$ we have to remember that Eq. (3.5) is written in the $|\boldsymbol{k}\rangle$ basis

$$\mathcal{H}_{\mathrm{BHZ}} = \int \mathrm{d}\boldsymbol{k}\; |\boldsymbol{k}\rangle\, H_{\mathrm{BHZ}}(\boldsymbol{k})\, \langle \boldsymbol{k}| \tag{4.5}$$

and that K also acts on this basis:

$$\begin{aligned} K\,|\boldsymbol{k}\rangle = K \int \mathrm{d}\boldsymbol{x}\; |\boldsymbol{x}\rangle\, \mathrm{e}^{\mathrm{i}\boldsymbol{k}\boldsymbol{x}} &= \int \mathrm{d}\boldsymbol{x}\; |\boldsymbol{x}\rangle\, \langle \boldsymbol{x}\,|\, -\boldsymbol{k}\rangle\, K \\ &= |-\boldsymbol{k}\rangle\, K\,. \end{aligned} \tag{4.6}$$

Now we can easily check that Eq. (3.5) is indeed time-reversal invariant

$$\begin{aligned} T_{4\text{x}4}\mathcal{H}_{\mathrm{BHZ}}T_{4\text{x}4}^{-1} &= \int \mathrm{d}\boldsymbol{k}\; |\boldsymbol{k}\rangle\, U H^*_{\mathrm{BHZ}}(-\boldsymbol{k}) U^\dagger\, \langle \boldsymbol{k}| \\ &= \mathcal{H}_{\mathrm{BHZ}}\,. \end{aligned} \tag{4.7}$$

From this line we can also immediately see the degeneracy of $|\psi_\uparrow\rangle = (a, b, 0, 0)$ and $|\psi_\downarrow\rangle = (0, 0, a, b)$ since $T_{4\text{x}4}\left|\psi_\uparrow\right\rangle = -\left|\psi_\downarrow^*\right\rangle$ and if $\mathcal{H}_{\mathrm{BHZ}}\,|\psi_\uparrow\rangle = E\,|\psi_\uparrow\rangle$ then

$$E = \left\langle \psi_\uparrow \right| T_{4\text{x}4}^{-1} T_{4\text{x}4}\mathcal{H}_{\mathrm{BHZ}} T_{4\text{x}4}^{-1} T_{4\text{x}4} \left|\psi_\uparrow\right\rangle \equiv \langle \psi_\downarrow |\, \mathcal{H}_{\mathrm{BHZ}}\, |\psi_\downarrow\rangle\,. \tag{4.8}$$

So $|\psi_\uparrow\rangle$ and $|\psi_\downarrow\rangle$ are degenerate in energy. In a similar fashion, we want to apply $T_{4\text{x}4}$ on both layers which shouldn't influence the layer pseudospin. This can be simply accomplished by a Kronecker product with $\mathcal{P}_0$. To obtain an order

which allows for a compact notation and handling of the resulting Hamiltonian, we choose $T_{8x8} = \mathrm{i}(\sigma_2 \otimes \mathcal{P}_0 \otimes \sigma_0)K$. The Hamiltonian

$$H_{\mathrm{DQW}}(\boldsymbol{k}) = \begin{pmatrix} H^{\uparrow}(\boldsymbol{k}) & \\ & H^{\downarrow}(\boldsymbol{k}) \end{pmatrix}, \qquad H^{\downarrow}(\boldsymbol{k}) = H^{\uparrow}(-\boldsymbol{k})^* \tag{4.9}$$

preserves the expected TRS: $T_{8x8}\mathcal{H}_{\mathrm{DQW}}T_{8x8}^{-1} = \mathcal{H}_{\mathrm{DQW}}$. To be clear, the ordered basis of this Hamiltonian is

$$\Big(|U, E1+\rangle, |U, H1+\rangle, |L, E1+\rangle, |L, H1+\rangle, \\ |U, E1-\rangle, |U, H1-\rangle, |L, E1-\rangle, |L, H1-\rangle \Big). \tag{4.10}$$

Rashba-like tunneling terms between different spins like $\langle U, E1+ | H | L, E1- \rangle$ were neglected in this model. They are qualitatively not important as long as they are smaller than the bulk gap and lead only to a small tilting of the bulk dispersion curves, see supplementary material of Ref. [10]. Bulk means here that it's not the $E(\boldsymbol{k})$ dispersion of the edge states.

4.2 Landau levels

We want to apply a magnetic field in the z direction with the same substitutions as in Section 3.2. As we know from Eq. (3.11), $h(\boldsymbol{k}) \to h_+$ and $h^*(-\boldsymbol{k}) \to h_-$. By using these substitutions, we obtain

$$\boldsymbol{\Delta}(\boldsymbol{k}) \cdot \boldsymbol{\sigma} \to \Delta\sigma_+, \qquad \boldsymbol{\Delta}^*(-\boldsymbol{k}) \cdot \boldsymbol{\sigma} \to \Delta\sigma_-, \\ \Delta\sigma_+ = \begin{pmatrix} \Delta_{E1E1} & \frac{\sqrt{2}\alpha}{l_B} a^\dagger \\ \frac{\sqrt{2}\alpha}{l_B} a & \Delta_{H1H1} \end{pmatrix}, \tag{4.11}$$

and $\Delta\sigma_-$ with the same diagonal terms and the negative complex conjugate on the offdiagonal, just like in the case of Eq. (3.11). In total we obtain:

$$H_{DQW} \to \begin{pmatrix} H_+ & \\ & H_- \end{pmatrix}, \tag{4.12}$$

where

$$H_\pm = \begin{pmatrix} h_\pm + V/2 & \Delta\sigma_\pm/2 \\ \Delta\sigma_\pm/2 & h_\pm - V/2 \end{pmatrix}. \tag{4.13}$$

We solve these decoupled matrices independently. The ansatz for $n > 0$, applied for each layer, also holds here

$$|\psi_+\rangle = \begin{pmatrix} a_+ |n\rangle \\ b_+ |n-1\rangle \\ c_+ |n\rangle \\ d_+ |n-1\rangle \end{pmatrix} \quad \text{and} \quad |\psi_-\rangle = \begin{pmatrix} a_- |n-1\rangle \\ b_- |n\rangle \\ c_- |n-1\rangle \\ d_- |n\rangle \end{pmatrix}. \tag{4.14}$$

This time the two resulting algebraic 4x4 matrices $H_\pm$ are in general not analytically solvable:

$$H_\pm = \begin{pmatrix} M - \frac{2(D+B)}{l_B^2}\left(n \pm \frac{1}{2}\right) + \frac{V}{2} & \pm\frac{\sqrt{2}A}{l_B}\sqrt{n} & \cdots \\ \pm\frac{\sqrt{2}A}{l_B}\sqrt{n} & -M - \frac{2(D-B)}{l_B^2}\left(n \mp \frac{1}{2}\right) + \frac{V}{2} & \\ \Delta_{E1E1} & \pm\frac{\sqrt{2}\alpha}{l_B}\sqrt{n} & \\ \pm\frac{\sqrt{2}\alpha}{l_B}\sqrt{n} & \Delta_{H1H1} & \end{pmatrix}$$

$$\begin{pmatrix} \cdots & \Delta_{E1E1} & \pm\frac{\sqrt{2}\alpha}{l_B}\sqrt{n} \\ & \pm\frac{\sqrt{2}\alpha}{l_B}\sqrt{n} & \Delta_{H1H1} \\ \cdots & M - \frac{2(D+B)}{l_B^2}\left(n \pm \frac{1}{2}\right) - \frac{V}{2} & \pm\frac{\sqrt{2}A}{l_B}\sqrt{n} \\ & \pm\frac{\sqrt{2}A}{l_B}\sqrt{n} & -M - \frac{2(D-B)}{l_B^2}\left(n \mp \frac{1}{2}\right) - \frac{V}{2} \end{pmatrix}. \tag{4.15}$$

Of course we can numerically solve it for given parameters. For an analytical solution one can try to neglect the smallest factor which are the off-diagonal terms of Eq. (4.11). However, this results in a very long expression for the energy of the LLs. If we would neglect even Δ_{E1E1} to reduce complexity, we arrive at the case of very weak coupling, where all tunnneling go to zero and which is discussed later on. Keep in mind that the two layers are indistinguishable since the tunneling is absolutely symmetric. Therefore the system is invariant under exchange of the layers and exchange of the sign of V and $\mathcal{B}$. Hence we will only regard $V > 0$ without loss of generality.

Now, we want to derive the zero modes $n = 0$ of this system. We can use the fact that Δ_{H1H1} is much smaller than all the other parameters and can be set to zero as pointed out in Ref [10]. Therefore, we can assume that for spin down the zero

modes are either on the upper or the lower layer:

$$\left|\psi_{-}^{U}\right\rangle = \begin{pmatrix} 0 \\ |0\rangle \\ 0 \\ 0 \end{pmatrix} \quad \text{and} \quad \left|\psi_{-}^{L}\right\rangle = \begin{pmatrix} 0 \\ 0 \\ 0 \\ |0\rangle \end{pmatrix} \tag{4.16}$$

which gives

$$E_{-}^{U/L} = -M - \frac{D-B}{l_B^2} \pm \frac{V}{2}\,. \tag{4.17}$$

These are the energies of a single layer shifted by $\pm V/2$. Due to the tunneling Δ_{E1E1} we can't assume this localization for spin up. Instead we make a more general ansatz

$$|\psi_{+}\rangle = \begin{pmatrix} \kappa\,|0\rangle \\ 0 \\ \lambda\,|0\rangle \\ 0 \end{pmatrix} \tag{4.18}$$

which results in a rather simple matrix

$$H_{+}\,|\psi_{+}\rangle = \begin{pmatrix} M - \frac{D+B}{l_B^2} + \frac{V}{2} & & \Delta_{\mathrm{E1E1}}/2 & \\ & -M - \frac{D-B}{l_B^2} + \frac{V}{2} & & \\ \Delta_{\mathrm{E1E1}}/2 & & M - \frac{D+B}{l_B^2} - \frac{V}{2} & \\ & & & -M - \frac{D-B}{l_B^2} - \frac{V}{2} \end{pmatrix} |\psi_{+}\rangle\,. \tag{4.19}$$

With the constraint that the eigenvectors have to be consistent with the ansatz in Eq. (4.18), i.e. the $H1$ components are zero, we obtain the two possible eigenvalues

$$E_{+}^{1/2} = M - \frac{D+B}{l_B^2} \pm \frac{\sqrt{V^2 + \Delta_{\mathrm{E1E1}}^2}}{2}\,. \tag{4.20}$$

These eigenvalues show again that $V \to -V$ leaves the system invariant. Furthermore we have reproduced the energy levels for $\boldsymbol{k} = 0$ [10] if we set $\mathcal{B} \to 0 \Leftrightarrow l_B \to \infty$. Note that at this point the ratio of the weight of the eigenvectors $q_{1/2} = \left|\kappa_{1/2}\right|^2 / \left|\lambda_{1/2}\right|^2 = 1$ which means that the eigenvectors of the E1 zero modes are equally spread over both layers. For a barrier thickness of $t = 5\,\mathrm{nm}$

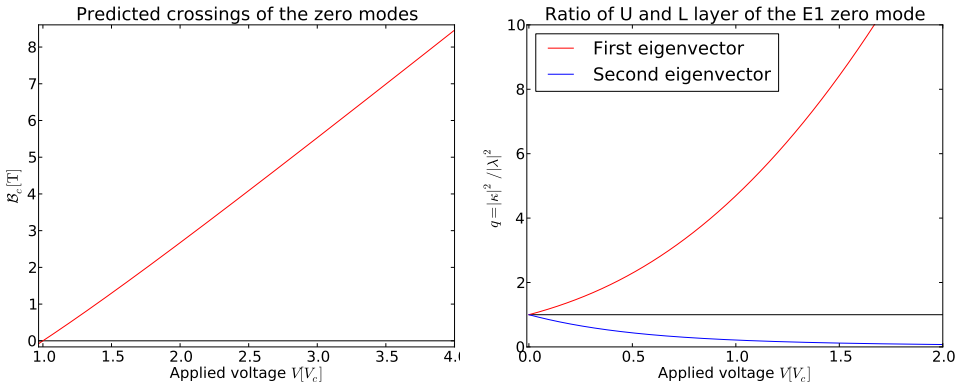

Figure 4.3: The left picture shows Eq. (4.22) for a barrier of $t = 5\,\text{nm}$, the parameters are given in Section 4.2. The critical voltage for this system is given by Eq. (4.23) and has a value of $V_c = 10.23\,\text{meV}$. The right picture shows the ratio of the upper and lower layer. $q \to (\infty, 0)$ corresponds to fully seperated layers.

the tunneling parameters are $\alpha = 10\,\text{meV}\,\text{nm}$ and $\Delta_{E1E1} = 12\,\text{meV}$ [10]. The dependence of the eigenvectors on the applied voltage is shown in Fig. 4.3. As in the case of the single layer the weight of the zero modes does not depend on the magnitude of the magnetic field. For increasing V, the eigenvectors are either on the upper or the lower layer. Of course this is expected because V seperates the energy levels sufficiently to neglect the coupling Δ_{E1E1}. Fig. 4.3 is representative for all possible tunneling parameters and inverted as well as noninverted layers. In the case of a stronger coupling, one only has to apply a higher voltage to seperate the layers.

4.3 Crossing of zero modes

Because we have studied the crucial importance of the zero modes for the behaviour of the system in the single layer we should analyze when these lines cross and what we can expect there. Of course E_+^1 (E_-^U) can't cross E_+^2 (E_-^L) since they are only shifted and have the same slope. Possible crossings are

$$\begin{aligned} \mathcal{B}_c^{1U/L} &= \frac{4M \mp V - \sqrt{V^2 + \Delta_{E1E1}^2}}{4eB}, \\ \mathcal{B}_c^{2U/L} &= \frac{4M \mp V + \sqrt{V^2 + \Delta_{E1E1}^2}}{4eB}, \end{aligned} \tag{4.21}$$

where $\mathcal{B}_c^{1U}$ is the magnetic field where a crossing between E_+^1 and E_-^U occurs. The concrete double layer geometry plays only a minor role here. Different values for Δ_{E1E1} only change the concrete value of V for which the crossing appears. Since $B < 0$ the numerator of Eq. (4.21) should be negative as well for a finite $\mathcal{B}_c$. If we use two quantum wells in the normal regime, we have $M > 0$. Therefore $\mathcal{B}_c^{2U/L}$ has no positive value. We are left with $\mathcal{B}_c^{1U/L}$ which can be tuned by V. However only for $4M < \Delta_{E1E1}$ we have two solutions. This would mean a very strong coupling where the presented DQW model Eq. (4.3) might not be valid any more. This is why we neglect this case at first and will analyze it afterwards in Section 4.4. The only remaining crossing is

$$\mathcal{B}_c^{1U} = \frac{4M - V - \sqrt{V^2 + \Delta_{E1E1}^2}}{4eB} \tag{4.22}$$

which only exists for $V > V_c$, for which the numerator of Eq. (4.22) becomes negative. To obtain V_c we set Eq. (4.22) equal zero:

$$V_c = 2M - \frac{\Delta_{E1E1}^2}{8M} \,. \tag{4.23}$$

This is exactly the same as V_c in Eq. (4.4) under the assumption that $\Delta_0 = \Delta_z \Leftrightarrow \Delta_{H1H1} \approx 0$ which we have used above as well. However, the authors of Ref. [10] have obtained V_c by looking for a change of sign in the local energy gap at $k = 0$ and had no magnetic field involved at all. Furthermore, they explicitely calculated Kramer's Chern numbers to verify that there is indeed a topological phase transition at V_c. We have derived the same critical condition for V by searching for a crossing of the zero modes. This shows that the existence of a crossing indicates a topological non-trivial behaviour of the system similar to the case of the single layer in Section 3.4. Although it is not yet clear how the topological behaviour for $\mathcal{B} = 0$ influences the concrete crossing point $\mathcal{B}_c$, we can conjecture that the mere existence of a crossing results from the nontrivial topology. While for the single layer the crossing in Eq. (3.17) was only depending on the material parameters M and B, Eq. (4.22) is tunable by the applied voltage V as shown in Fig. 4.3.

4.4 DQW with noninverted layers

We show now the LLs for noninverted layers with $M \approx 6.5\,\text{meV}$ which corresponds to a thickness of $d = 5.7\,\text{nm}$. This is the same thickness we have already examined in Chapter 3 where we have also given the parameters in Table 3.1.

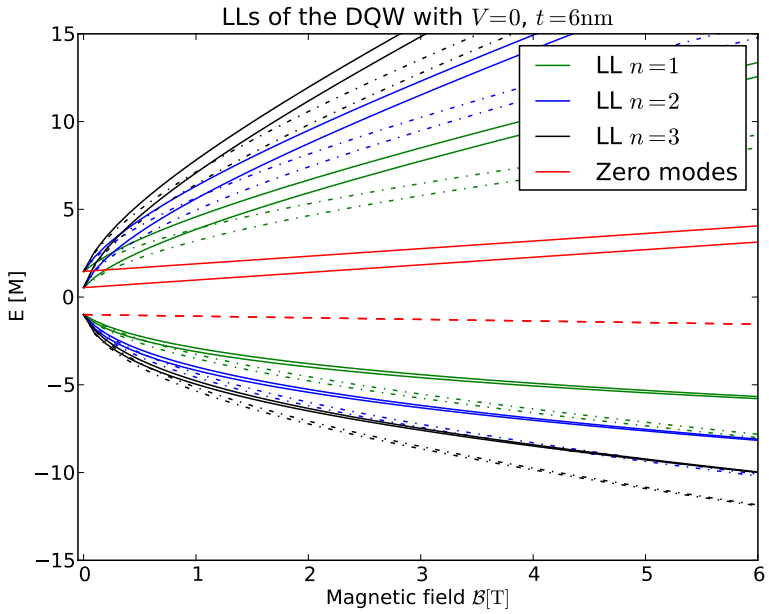

Figure 4.4: LL fan diagram of the DQW without interlayer voltage. As pointed out in the text, the $E_-^{U/L}$ zero modes fall in this case together. Since this line has H1 character, we draw it dashed. For the higher LLs we indicate the energies of H_+ (H_-) with solid (dash-dotted) lines. In this case, the system behaves as ordinary insulator if ϵ_F is placed in the gap.

Reasonable coupling $t = 6\,\text{nm}$

The tunneling parameters are given in Ref. [10]. To begin the discussion we look at the case $V = 0$. Here, the zero modes $E_-^{U/L}$ fall together and only three distinct zero modes remain. The possible crossing would occur at $\mathcal{B}_c^{1U} = (4M - |\Delta_{E1E1}|)/(4eB)$ which is negative in the regarded case. So there is no finite crossing point which is affirmed by Fig. 4.4 and the system acts as an ordinary insulator if ϵ_F is placed in between the zero modes. However, this is the easiest case to realize as one only has to short-circuit the two layers. Furthermore, this should

result in quite different Hall-Plateaus if we compare the LLs with Fig. 3.4. With the measuring approach described in Section 3.4, one should be able to see the splitting of the two energies $E_+^{1/2}$ which results from the tunneling term Δ_{E1E1}. On the other hand, the degenerated $E_-^{U/L}$ should give a a jump of two units in the Hall conductivity. This would mean an unusual type of QH effect which is different from the conventional integer QH effect or the one in bilayer or single layer graphene, shown in Ref. [30]. If we now turn on the interlayer voltage V, we

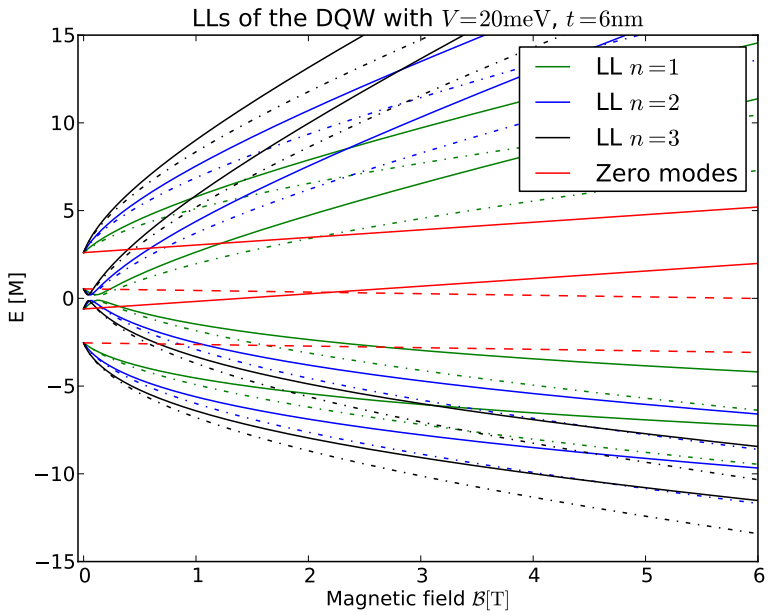

Figure 4.5: For the given parameters $V_c = 12.31\,\text{meV}$ and therefore we can see a crossing for $V = 20\,\text{meV}$ while all other parameters are the same as in Fig. 4.4. Close to $\mathcal{B} = 0$ we can see the coupling Δ_{E1E1} between upper and lower layer bands which results in the anti-crossing.

expect a splitting of $E_-^{U/L}$. The critical voltage for which the crossing enters is given by Eq. (4.23) and has a value of $V_c = 12.31\,\text{meV}$ for this system. In Fig. 4.5 we show a representative plot of the LLs for $V > V_c$ where the expected crossing can be seen. According to Ref. [10], we have a topologically nontrivial system here. Note that at $V = V_c$, a gapless system is created. In Fig. 4.5, we can also see which bands are coupled and show therefore an anti-crossing and which bands are not coupled. Solid and dash-dotted lines, which correspond to H_+ (H_-), can cross since we haven't included Rashba-like terms.

Strong coupling $4M \leq \Delta_{E1E1},\ t = 3\,\mathrm{nm}$

The results in this subsection should be regarded with a bit caution since the tunneling barrier is now half as thin as the width of the two QWs. In this case, the DQW model might not be valid any longer. A new crossing

$$\mathcal{B}_c^{1L} = (4M + V - \sqrt{V^2 + \Delta_{E1E1}^2})/(4eB) \tag{4.24}$$

appears now which is degenerated to $\mathcal{B}_c^{1U}$ for V=0: $\mathcal{B}_c^{1U/L} = (4M - |\Delta_{E1E1}|)/(4eB)$. This is related to the degenerated $E_-^{U/L}$. For all voltages we have now at least one crossing. Since we are in the regime of strong coupling, the system is topologically nontrivial for all voltages which can be seen by a look at Fig. 4.2 at $\Delta_z \geq 2M$. Therefore, there is no critical V_c for which a phase transition might appear. By increasing V, we are only removing the degeneracy of $E_-^{U/L}$ which allows us to see in Fig. 4.6 a double crossing. However, this second crossing is never in the bulk insulating gap. Because of the negative slope of $E_-^{U/L}$, the second crossing point is always below the gap. Furthermore, due to the value of the Chern number there is only one edge state [10]. It is important to note that two crossing don't imply that two edge states are existing. But the nontrivial topological insulator phase is affirmed by the overall existing crossing point in the gap. For voltages above $V \approx 20\,\mathrm{meV}$, the second crossing disappears, like it is shown in Fig. 4.7.

Very weak coupling $t \to \infty$

If the tunneling barrier is very thick, we have two copies of the BHZ model which have an offset due to the interlayer voltage. In this case, all coupling constants go to zero and the LLs are described by Eq. (3.14) $\pm V/2$. We have to be careful with Eq. (4.22) and Eq. (4.23) which would suggest a nontrivial behaviour. But in this case the crossing has no meaning. It is only a relocation of the energy levels and the crucial ingredient of a coupling between the layers is missing. The behaviour is completely determined by the single layer discussion in Chapter 3.

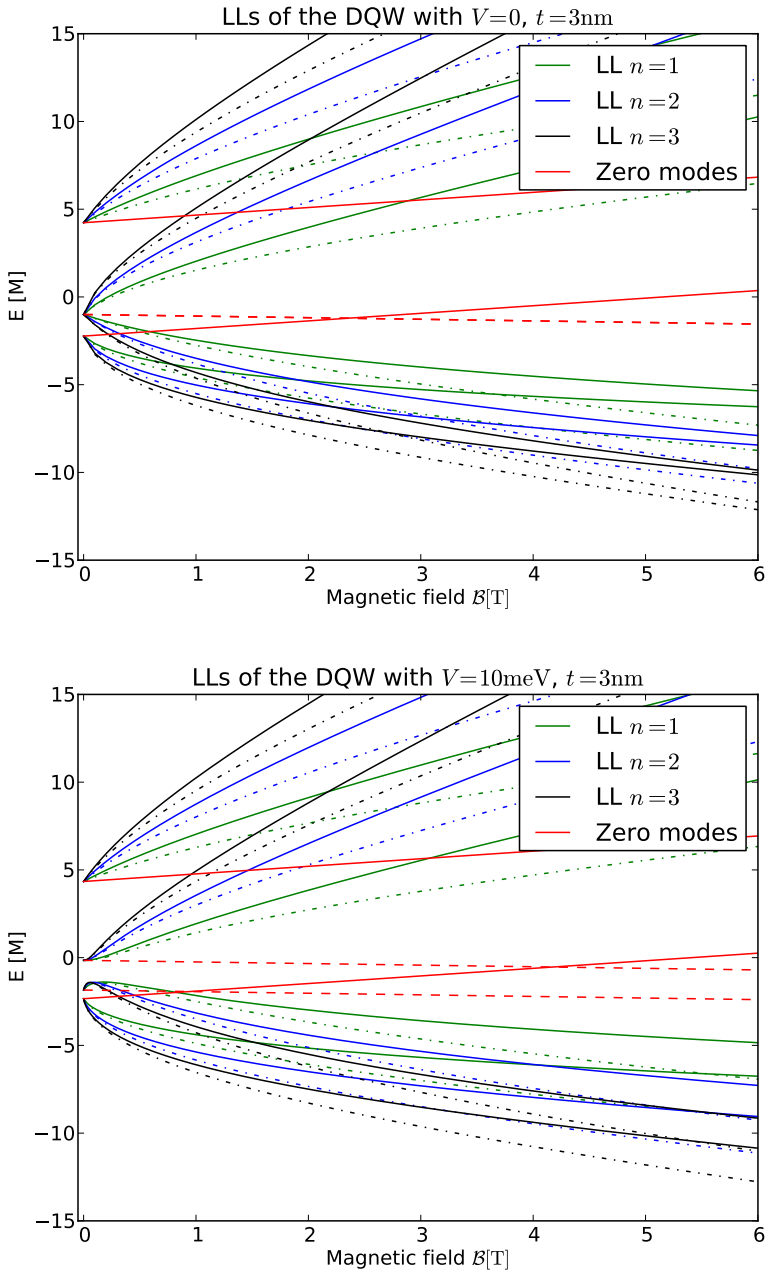

Figure 4.6: The Landau levels for strong coupling show a crossing even for $V = 0$ and allow a double crossing for finite V. But this second crossing is not energetically seperated like the first and might be not seen in experiment at all. Linestyles are the same as before.

4.5 Comparsion with the reduced model $V \approx \pm 2M$

Inspired by bilayer graphene, Michetti *et al.* have shown further that if the relevant energies are small compared to $V \approx \pm 2M$ the system can be described by a reduced low-energy Hamiltonian $\tilde{h}_{ll}$ [10]. This Hamilton can be mapped to Eq. (3.5) with the following parameters

$$\begin{aligned} \tilde{A} &= \frac{\alpha}{2} \pm \frac{A\Delta_z}{M \pm \frac{V}{2}}, \quad \tilde{M} = M \mp \frac{V}{2} - \frac{\Delta_0^2 + \Delta_z^2}{4(M \pm \frac{V}{2})}, \\ \tilde{B} &= B - \frac{A^2}{M \pm \frac{V}{2}}, \quad \tilde{C} = C - \frac{\Delta_0 \Delta_z}{2(M \pm \frac{V}{2})} \quad \text{and} \quad \tilde{D} = D. \end{aligned} \tag{4.25}$$

Let us examine if this reduced model generates the same LLs as the full model at least in an area which is close to $\mathcal{B} = 0$. We cannot expect that the reduced model works for large magnetic fields because there the energy levels get close to each other and the assumptions made that lead to the reduced model are not fullfilled any more. Since the other energies should be small compared to $V \approx 2M = 13\,\text{meV}$ we expect the best results for a weak coupling like $t = 7\,\text{nm}$. For $V = 13\,\text{meV}$, we can expect a crossing of zero modes at $\mathcal{B}_c = 0.064\,\text{T}$. In Fig. 4.8, we have plotted both models. Although we have taken only a very close area around $\mathcal{B} = 0$, the LLs are already remarkably different from each other. In spite of that, the existence of a crossing is reproduced in the reduced model, only the concrete value of $\mathcal{B}_c$ isn't correct. This is affirmed by the topological considerations in Ref. [10]. The reduced model can be seen as a first order correction of two decoupled BHZ models. It should only be regarded for weak coupling and even there one should keep in mind that the LLs are not correctly reproduced. The phenomenon of double crossings which arise for strong coupling can not be understood in the single layer picture.

4.6 DQW with inverted layers

For the case of two inverted layers, we assume that the tunneling parameters are the same for $M \to -M_0$. Let us consider the possible crossings in Eq. (4.21). In this case, the two layers are topologically nontrivial and show crossings even without coupling. With $M < 0$, also $\mathcal{B}_c^{2U/L}$ is possible now. Therefore, in general there are up to four crossings. If $V = 0$ and $\Delta_{E1E1} = 0$, all four crossings are

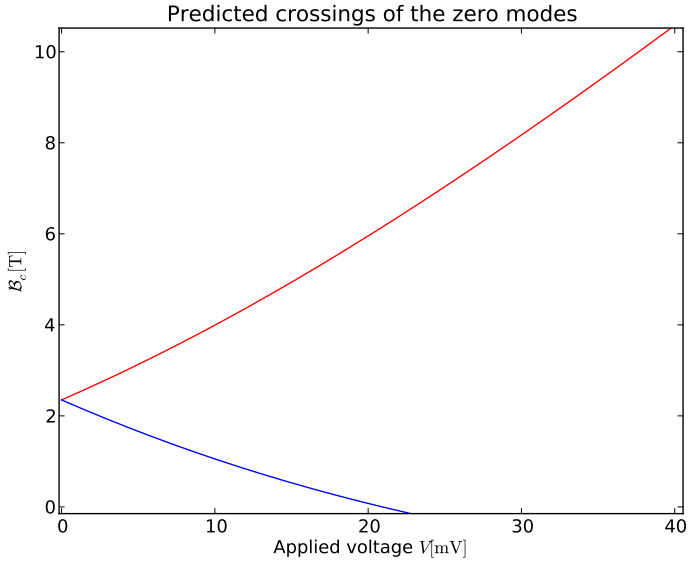

Figure 4.7: The two predicted crossings in the case of strong coupling $4M \leq \Delta_{E1E1}$ which corresponds to $t = 3\,\text{nm}$ for two QWs with $d = 5.7\,\text{nm}$. For voltages above $V \approx 20\,\text{meV}$ the second crossing gets destroyed again.

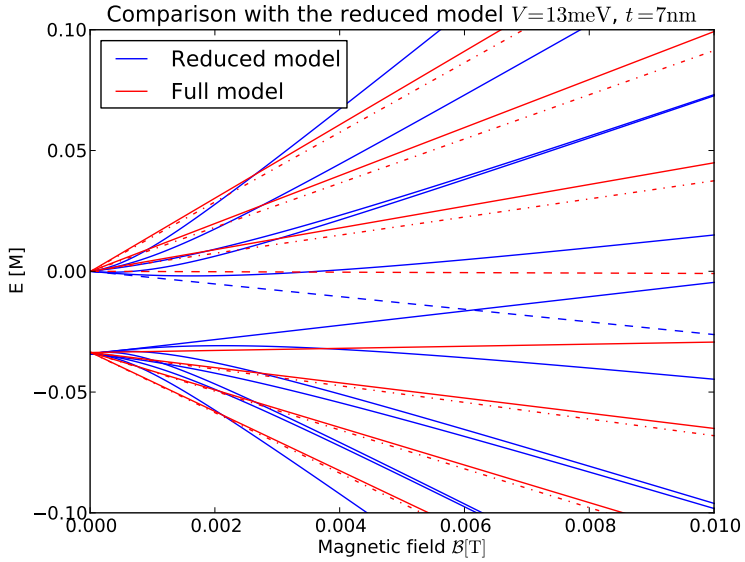

Figure 4.8: The reduced model shows the expected crossing but can't reproduce the correct value of $\mathcal{B}_c$. The crossing point of the full model is not included in this frame anymore. The other bands of the full model are not shown and start around $\pm 2M$ for $\mathcal{B} = 0$.

degenerated to the crossing of a single layer: $\mathcal{B}_c = M/(eB)$. Furthermore, we can note that for $V = 0$ only two crossings are possible due to the degenerated $E_-^{U/L}$ and for $\Delta_{E1E1} = 0$ there are three possibilities as one can see immediately from Eq. (4.21). The general behaviour is shown in Fig. 4.9. Interestingly, an increasing coupling destroys $\mathcal{B}_c^{2U/L}$ which is inherited from the inverted single layer. In order to see four crossings we have a look at $t = 7\,\mathrm{nm}$ in Fig. 4.10. For all possible voltages and couplings we have at least two crossings. The understanding of a DQW which consists of inverted layers is a bit cumbersome because there are different contributing phenomenona. There are the crossings which come from the inverted single layers as well as the crossings which arise from coupling and the inversion of bands due to V.

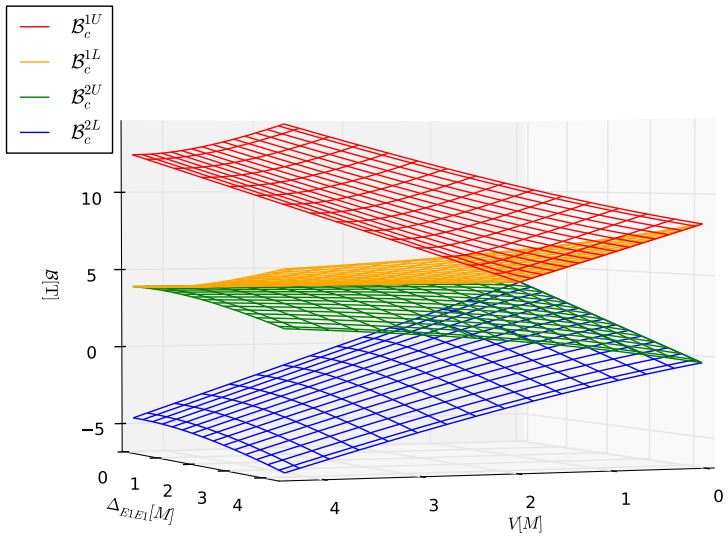

Figure 4.9: The calculated crossings for two inverted layers with the values of Table 3.1 and $M = -M_0$. The concrete number of crossings depends on the voltage and the coupling. If $\mathcal{B}_c$ is smaller than zero the crossing won't appear. In all cases we can expect at least two crossings.

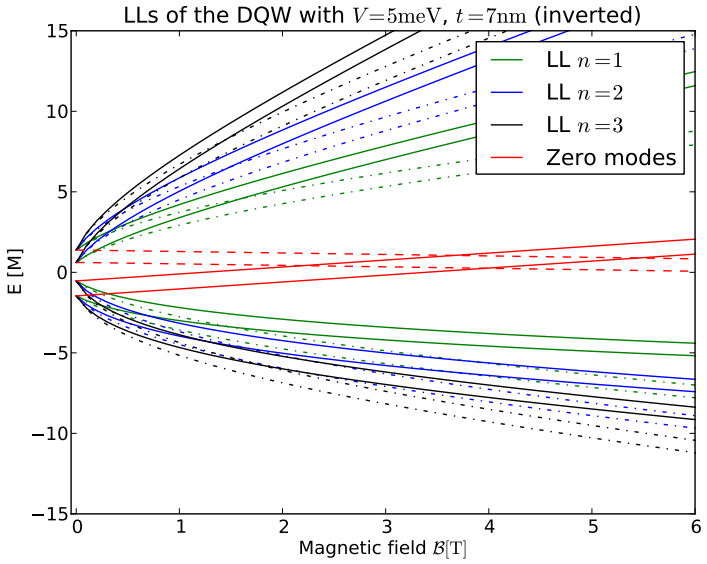

Figure 4.10: The LLs of the inverted layers show four crossings for weak coupling. The inverted orientation of the $E1$ and $H1$ zero modes is similar to Fig. 3.4.

5 Conclusion

This bachelor thesis provided the theoretical calculation of the Landaus levels (LLs) of the double quantum well (DQW) model of CdTe/HgTe by means of the Peierl's substitution. At first we motivated, how one can arrive at an effective multi-band description of heterostrucutures and in particular the Bernevig, Hughes, and Zhang (BHZ) model. We learned, that the LL fans of the materials represented by the BHZ model (CdTe,HgTe) show no simple dispersion with respect to the magnetic field like the free electron gas (linear) or graphene ($\sqrt{n\mathcal{B}}$). Furthermore, the crossing of zero modes ($n = 0$) have proven to be a visualization of the inverted band structure and indicate therefore, if the system behaves topologically trivial or nontrivial.

After understanding the LLs of the single layer, we moved on to analyze the DQW and it's promising feature, to change the topological insulator phase depending on the applied interlayer voltage which is on the order of the bandgap. We extended the DQW-BHZ model to both Kramer's blocks by use of time-reversal symmetry (TRS) and applied the magnetic field. Although the two resulting 4x4 matrices were analytically not solvable and show quite complex LL fan diagrams, the zero modes inherited the linear dispersion of the single layer. They revealed in particular, that the condition of the existence of a crossing leads in the regime of a reasonable coupling to the same criterion for the critical voltage, as the topological phase transition of the calculated Kramer's Chern number in Ref. [10]. By exploring the parameter space, we identified the regime of strong coupling $4M \leq \Delta_{E1E1}$ which shows a double crossing. The second crossing however was not in the bulk gap and does not correspond to a second edge channel. The double crossing does further not imply that the DQW is topologically trivial.

The DQW proposal should be experimentally quite feasible since each well is made of the same material and the width of the wells as of the tunneling barrier lies only between three and eight nanometres. The measurement of the Hall conductivity is an easy way to experimentally verify the predicted properties. Especially the case of short-circuited layers would in the strongly coupled as well as in the reasonably coupled case, which results in an unusual type of quantum Hall (QH) effect as pointed out in Section 4.4, be a good place to start.

Zusammenfassung

In dieser Bachelorarbeit wurde auf der Basis der Peierl's Substitution die theoretische Berechnung der Landau Levels (LLs) eines doppelten Quantentrogmodells (DQW) aus CdTe/HgTe durchgeführt. Zunächst wurde motiviert, wie man Heterostrukturen mit Hilfe von effektiven Multi-Band-Hamiltonians wie dem Bernevig, Hughes, und Zhang (BHZ) Modell beschreiben kann. Es hat sich herausgestellt, dass die LLs von Materialien, die durch das BHZ Modell beschrieben werden (CdTe, HgTe), keine einfache Dispersionsrelation bezüglich des Magnetfeldes aufweisen, im Vergleich zum freien Elektronengas (linear) oder Graphen ($\sqrt{n\mathcal{B}}$). Ferner konnten die Kreuzungen von Nullmoden ($n = 0$) als Visualisierung der invertierten Bandstruktur identifiziert werden, welche somit anzeigen, ob sich das System topologisch trivial oder nicht trivial verhält.

Mit dem Verständnis der LLs der Einzelschichten wurde der DQW und seine vielversprechende Eigenschaft, die topologische Phase abhängig von der Spannung (in der Größenordnung der Bandlücke) zu verändern, untersucht. Hierzu wurde das DQW-BHZ Modell mittels Zeitumkehrsymmetrie auf beide Kramer's Blöcke erweitert und das Magnetfeld angelegt. Obwohl die resultierenden 4x4 Matrizen nicht analytisch lösbar waren und relativ komplexe LLs zeigen, haben die Nullmoden weiterhin eine lineare Dispersion. Es hat sich insbesondere gezeigt, dass die Bedingung, dass eine Kreuzung von Nullmoden existiert, im Bereich gewöhnlicher Kopplung zum selben Kriterium für die kritische Spannung führt, wie der topologische Phasenübergang der berechneten Kramer's Chern Zahl in Ref. [10]. Bei der Untersuchung des Parameterraums wurde ein Bereich starker Kopplung $4M \leq \Delta_{E1E1}$ identifiziert, in dem zwei Kreuzungen auftreten. Die zweite Kreuzung liegt aber nicht in der Bandlücke und entspricht auch keinem zweiten Randkanal. Ferner implizieren zwei Kreuzungspunkte nicht, dass das DQW System topologisch trivial ist.

Der Vorschlag eines DQW sollte experimentell gut realisierbar sein, da jeder Quantentrog aus demselben Material besteht und die Dicke der Schichten nur zwischen drei und acht Nanometer liegt. Die Messung der Hallleitfähigkeit stellt eine einfache Möglichkeit dar, die vorhergesagten Eigenschaften experimentell zu verifizieren. Insbesondere der Fall von kurzgeschlossenen Schichten wäre sowohl im

Bereich starker als auch mäßiger Kopplung, die in einem ungewöhnlichem Quantenhalleffekt resultiert, wie in Section 4.4 gezeigt wurde, ein guter Anhaltspunkt.

Bibliography

[1] K. von Klitzing. The quantized hall effect. *Rev. Mod. Phys.*, 58:519–531, Jul 1986.

[2] D. J. Thouless, M. Kohmoto, M. P. Nightingale, and M. den Nijs. Quantized hall conductance in a two-dimensional periodic potential. *Phys. Rev. Lett.*, 49:405–408, Aug 1982.

[3] X.-L. Qi and S.-C. Zhang. Topological insulators and superconductors. *Rev. Mod. Phys.*, 83:1057–1110, Oct 2011.

[4] S. Raghu. *Topological aspects of systems with broken time-reversal symmetry.* PhD thesis, Princeton University, 2006.

[5] C. L. Kane and E. J. Mele. Z_2 topological order and the quantum spin hall effect. *Phys. Rev. Lett.*, 95:146802, Sep 2005.

[6] B. A. Bernevig, T. Hughes, and S.-C. Zhang. Quantum Spin Hall Effect and Topological Phase Transition in HgTe Quantum Wells. *Science*, 314(5806):1757–1761, 2006.

[7] M. König, H. Buhmann, L. W. Molenkamp, T. Hughes, C.-X. Liu, X.-L. Qi, and S.-C. Zhang. The Quantum Spin Hall Effect: Theory and Experiment. *Journal of the Physical Society of Japan*, 77(3):031007, 2008.

[8] Markus König, Steffen Wiedmann, Christoph Brüne, Andreas Roth, Hartmut Buhmann, Laurens W. Molenkamp, Xiao-Liang Qi, and Shou-Cheng Zhang. Quantum spin hall insulator state in hgte quantum wells. *Science*, 318(5851):766–770, 2007.

[9] APS. Oliver E. Buckley Condensed Matter Prize. `http://www.aps.org/programs/honors/prizes/buckley.cfm`, April 2012.

[10] P. Michetti, J. C. Budich, E. G. Novik, and P. Recher. Tunable quantum spin hall effect in double quantum wells. *Phys. Rev. B*, 85:125309, Mar 2012.

[11] N. W. Ashcroft and N. D. Mermin. *Festkörperphysik.* Oldenbourg, 2001.

[12] G. Czycholl. Chap. 4. In *Theoretische Festkörperphysik: Von den klassischen Modellen zu modernen Forschungsthemen*. Springer, 2007.

[13] C. Cohen-Tannoudji, B. Diu, and F. Laloe. Chap. 11. In *Quantenmechanik*.

[14] E. O. Kane. Chap. 3: The $\boldsymbol{k} \cdot \boldsymbol{p}$ method. In *Semiconductors and semimetals, 1*. Academic Press, 1966.

[15] Jasprit Singh. *Electronic and Optoelectronic Properties of Semiconductor Structures*. Cambridge University Press, 2003.

[16] F. Schwabl. Chap. 5.3.5.4. In *Quantenmechanik für Fortgeschrittene (QM II)*. Springer, 2008.

[17] J. M. Luttinger and W. Kohn. Motion of electrons and holes in perturbed periodic fields. *Phys. Rev.*, 97:869–883, Feb 1955.

[18] W. Miller. Lemma 5.3. In *Symmetry groups and their applications, Volume 50 (Pure and Applied Mathematics)*. Academic Press, 1972.

[19] R. Peierls. Zur Theorie des Diamagnetismus von Leitungselektronen. *Zeitschrift für Physik A Hadrons and Nuclei*, 80:763–791, 1933.

[20] E. O. Kane. Band structure of indium antimonide. *Journal of Physics and Chemistry of Solids*, 1(4):249 – 261, 1957.

[21] A. Pfeuffer-Jeschke. *Bandstruktur und Landau-Niveaus quecksilberhaltiger II-VI-Heterostrukturen*. PhD thesis, JMU Würzburg, 2000.

[22] E. G. Novik, A. Pfeuffer-Jeschke, T. Jungwirth, V. Latussek, C. R. Becker, G. Landwehr, H. Buhmann, and L. W. Molenkamp. *Phys. Rev. B*, 72, Jul 2005.

[23] M. G. Burt. Fundamentals of envelope function theory for electronic states and photonic modes in nanostructures. *Journal of Physics: Condensed Matter*, 11(9):53, 1999.

[24] P. Capper. A2.2 Lattice parameter of HgCdTe. In *Properties of Narrow Gap Cadmium-Based Compounds (emis Datareviews Series)*. The Institution of Engineering and Technology, 1994.

[25] M. O. Goerbig. Electronic properties of graphene in a strong magnetic field. *Rev. Mod. Phys.*, 83:1193–1243, Nov 2011.

[26] Z. F. Ezawa. Chap. 10 Landau quantization. In *Quantum Hall Effects: Field Theorectical Approach and Related Topics*. World Scientific Publishing Company, 2008.

[27] B. Büttner, C. X. Liu, G. Tkachov, E. G. Novik, C. Brüne, H. Buhmann, E. M. Hankiewicz, P. Recher, B. Trauzettel, S. C. Zhang, and L. W. Molenkamp. Single valley dirac fermions in zero-gap hgte quantum wells. *Nat Phys*, 7(5):418–422, May 2011.

[28] S. Weinberg. *The Quantum Theory of Fields, Volume 1: Foundations*. Cambridge University Press, 2005.

[29] J. J. Sakurai. *Modern Quantum Mechanics (Revised Edition)*. Addison Wesley, 1993.

[30] K. S. Novoselov, E. McCann, S. V. Morozov, V. I. Fal'ko, M. I. Katsnelson, U. Zeitler, D. Jiang, F. Schedin, and A. K. Geim. Unconventional quantum Hall effect and Berry's phase of 2π in bilayer graphene. *Nature Physics*, 2(3):177–180, February 2006.

Declaration

Hereby I declare the single handed composition of this thesis. Furthermore I confirm that no other sources have been used than those specified in the thesis itself. This thesis has not been submitted as part of another examination process neither in identical nor in similar form.

May 9, 2012